

Communication

A “Special” Solvent to Prepare Alloyed Pd₂Ni₁ Nanoclusters on a MWCNT Catalyst for Enhanced Electrocatalytic Oxidation of Formic Acid

Pingping Yang^{1,2,†}, Li Zhang^{1,2,†}, Xuejiao Wei¹, Shiming Dong¹, Wenting Cao¹, Dong Ma¹, Yuejun Ouyang¹, Yixi Xie^{2,*}  and Junjie Fei^{2,*}¹ College of Chemistry and Materials Engineering, Huaihua University, Huaihua 418008, China² College of Chemistry, Xiangtan University, Xiangtan 411105, China

* Correspondence: xieyixige@xtu.edu.cn (Y.X.); fei_junjie@xtu.edu.cn (J.F.)

† These authors contributed equally to this work.

Abstract: Herein, an electrocatalyst with Pd₂Ni₁ nanoclusters, supporting multiwalled carbon nanotubes (MWCNTs) (referred to Pd₂Ni₁/CNTs), was fabricated with deep eutectic solvents (DES), which simultaneously served as reducing agent, dispersant, and solvent. The mass activity of the catalyst for formic acid oxidation reaction (FAOR) was increased nearly four times compared to a Pd/C catalyst. The excellent catalytic activity of Pd₂Ni₁/CNTs was ascribed to the special nanocluster structure and appropriate Ni doping, which changed the electron configuration of Pd to reduce the d-band and to produce a Pd–Ni bond as a new active sites. These newly added Ni sites obtained more OH[−] to release more effective active sites by interacting with the intermediate produced in the first step of FAOR. Hence, this study provides a new method for preparing a Pd–Ni catalyst with high catalytic performance.

Keywords: Pd₂Ni₁ nanocluster; doping; Pd–Ni bond; deep eutectic solvents; formic acid oxidation reaction



Citation: Yang, P.; Zhang, L.; Wei, X.; Dong, S.; Cao, W.; Ma, D.; Ouyang, Y.; Xie, Y.; Fei, J. A “Special” Solvent to Prepare Alloyed Pd₂Ni₁ Nanoclusters on a MWCNT Catalyst for Enhanced Electrocatalytic Oxidation of Formic Acid. *Nanomaterials* **2023**, *13*, 755. <https://doi.org/10.3390/nano13040755>

Academic Editors: Arthur P. Baddorf and Francesc Viñes Solana

Received: 15 December 2022

Revised: 3 February 2023

Accepted: 12 February 2023

Published: 17 February 2023



Copyright: © 2023 by the authors. Licensee MDPI, Basel, Switzerland. This article is an open access article distributed under the terms and conditions of the Creative Commons Attribution (CC BY) license (<https://creativecommons.org/licenses/by/4.0/>).

1. Introduction

Liquid fuel cells are booming related to achieving carbon neutrality [1–5]. Direct formic acid fuel cell (DFAFC) is a kind of important fuel cell and attracts much attention [6–8]. However, low conversion efficiency of formic acid has always been a difficult problem. This is partly due to the slow kinetics of multi-electron transfer during the formic acid oxidation reaction (FAOR).

Palladium (Pd) is a kind of precious metal that has a good catalytic effect towards FAOR [9]. Besides, various Pd-based bimetallic alloy catalysts were prepared to improve the FAOR (e.g., PdAg [10], PdSn [11], PdNi [12], PdBi [13], and PdRu [14]). Among these alloy catalysts, PdNi binary catalysts have attracted much attention. Gao et al. [15] prepared a Pd–Ni/C catalyst that shows excellent performance for FAOR. Han et al. [16] fabricated Pd_xNi/rGO catalyst showing enhanced mass activity toward FAOR. The doping of the Ni is conducive to change the electronic structure around the Pd atom, which is conducive to improve the toxicity resistance of the catalyst. Although the addition of the second metal has improved the catalytic performance of the single Pd catalyst for formic acid to a certain extent, in order to meet practical application, the catalyst performance needs to be improved.

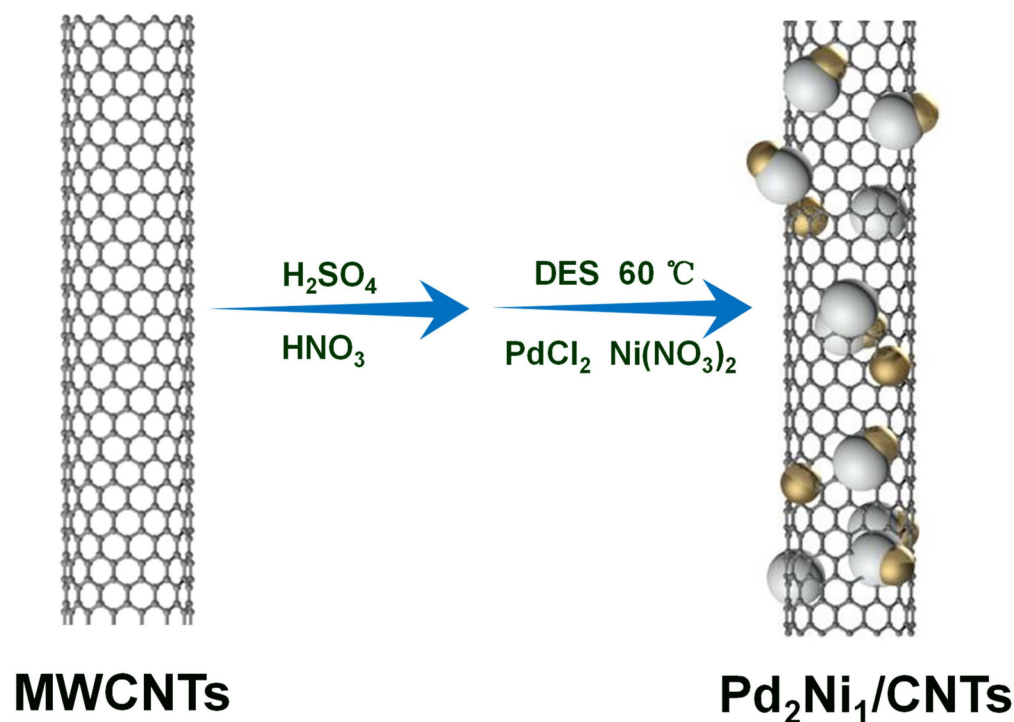
Optimizing the morphology of Pd binary catalysts is helpful to improve their catalytic performance. Among all kinds of heterogeneous structures, catalysts with nanocluster structures have attracted much attention. This structure generally has rough surfaces and abundant low-coordination atoms, leading to larger electrochemically active surface area (ECSA) and improved electrocatalytic performance [17]. Besides, PdNi alloy nanocluster catalysts have not yet been reported so far.

For precious metals, doping can improve their catalytic activity [18]. However, too large or too small of a doping ratio cannot obtain the best catalytic performance. Hence, it is of great significance to explore the appropriate doping ratio to obtain a catalyst with high performance.

Recently, carbon materials have been widely used as carriers due to their excellent electron transport ability [19]. Among these carbon materials, MWCNTs have attracted much attention in fuel cells [20]. Hence, in this study, we introduced MWCNTs as carriers to improve the electron transport capacity of Pd₂Ni₁ nanoclusters.

It is well known that smaller nanoparticles can increase ECSA for more effective active sites. Deep eutectic solvents (DES) are an analogue of ionic liquids, with many advantages, wide electrochemical window, high electroconductivity, non-toxicity, thermal stability, biodegradability, and negligible vapor pressure, in addition to other advantages [21]. Our group [19,22–25] has also concluded that this green solvent can effectively reduce the size of nanoparticles in previous research. In addition, some research groups have successfully prepared PdSn [26] and PdAg [27] catalysts in DES. Specially, Hammons research group [28] used DES to stabilize the resulting Pd nanoparticles. Therefore, DES is a potential solvent for fabrication of catalysts with excellent performance.

The highlight of this work is that the Pd₂Ni₁-CNTs catalyst was prepared in DES for the first time. In this study, porous Pd₂Ni₁ nanoclusters were obtained in DES, so as to obtain larger ESCA to provide more active sites and thus obtain greater catalytic activity. In addition, conventional PdNi-CNT catalysts are usually prepared in a water system or in toxic organic solvents, and additional reducing agents are needed. Besides, DES is a green and environmentally friendly solvent used in this study. It serves as a reducing agent, dispersant, and solvent simultaneously in the preparation of a catalyst. In this study, Pd₂Ni₁ alloy nanoclusters on a MWCNT catalyst was fabricated with a DES-assisted environment (Scheme 1). Subsequent electrochemical tests showed that the catalyst had good CO resistance and excellent catalytic activity for formic acid.



Scheme 1. Schematic illustration showing the preparation of Pd₂Ni₁/CNTs.

2. Results and Discussion

Figure 1a shows the XRD patterns of Pd₂Ni₁/CNTs and Pd/CNTs. The diffraction peak near 26° is caused by C(002) of the carrier [19,23]. Compared to the Pd diffraction

peaks of Pd/CNTs (39.2° , 44.8° , 66.5° , and 79.8°), the Pd peaks of Pd₂Ni₁/CNTs shifted to the higher 2θ values (39.5° , 45.3° , 66.6° , and 80.3°), suggesting the formation of alloy [29]. This result may be due to the fact that the radius of Ni is smaller than Pd, which compresses the lattice constant of Pd during doping [30]. This phenomenon is also strong evidence for the formation of alloys. Using Scherrer's equation [31] to calculate the average nanoparticles' sizes of Pd₂Ni₁/CNTs (3.6 nm) (Figure 1b) and Pd/CNTs (4.1 nm) (Figure S1), the small size of nanoparticles in Pd₂Ni₁/CNTs resulted in more effective catalytic active sites on the catalyst, which was also the main reason for its large ESCA in electrochemical tests.

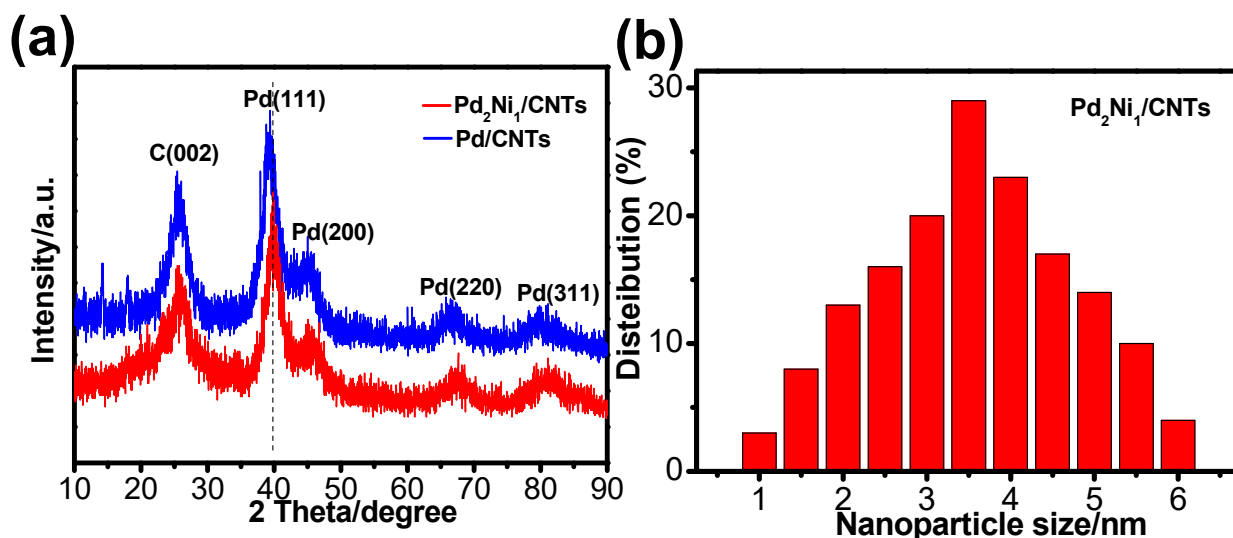


Figure 1. (a) XRD patterns of Pd/CNTs and Pd₂Ni₁/CNTs catalysts; (b) the corresponding particle size distribution of Pd₂Ni₁/CNTs.

Figure 2a–c show the TEM and HRTEM images of Pd₂Ni₁/CNTs. The Pd₂Ni₁ nanoclusters supported on MWCNTs are clear, and the spacing of Pd(111) crystal planes in Pd₂Ni₁/CNTs is 0.219 nm, while the value is (0.222 nm) in Pd/CNTs (Figure S2), providing further evidence of alloying [23]. It is clear that the nanoclusters are made up of smaller nanoparticles, with gaps between them that allow formic acid molecules to be transported through them and oxidized [32]. Figure 2d–g display the HAADF-STEM images of Pd and Ni, which are supported by the EDX line-profiles and spot scanning (Figure S3). It is clear that the Pd and Ni atoms appear in almost the same position. This grounding proves the presence of the alloy, and the cluster structure is also evident.

As shown in Figure 3a, the signal peaks corresponding to C1s, O1s, Pd3d, and Ni2p appear in the full spectrum of Pd₂Ni₁/CNTs. This indicates that the Pd₂Ni₁/CNTs catalyst has been successfully prepared. As can be seen from Figure 3b, the two C–C and C–O peaks are C1 peaks of MWCNTs-AO. After acidification, the surface of the originally smooth CNTs became rough and defective. Figure 3c shows the peaks of Ni2p (Ni 2p_{1/2} and Ni 2p_{3/2}). The Ni 2p_{3/2} spectra show the peaks at 856.0 and 860.8 eV, while the Ni 2p_{1/2} spectra show the peaks at 872.7 and 874.8 eV, accompanied with satellite peaks at 864.0 and 880.4 eV [33]. The presence of Ni⁰ and Ni⁺² is attributed to their alloy formation with Pd and further oxidation by exposure to air, respectively. As can be seen from Figure 3d, the peak position of Pd⁰ varied from Pd/CNTs to Pd₂Ni₁/CNTs by 0.2 eV (Table S1), indicating a strong charge transfer interaction between Ni and Pd [34]. The optimized Ni doping can effectively regulate the arrangement of the electron configuration of Pd and inhibit the CO_{ads} toxicity at active sites. This is also one of the important reasons for the improvement of performance.

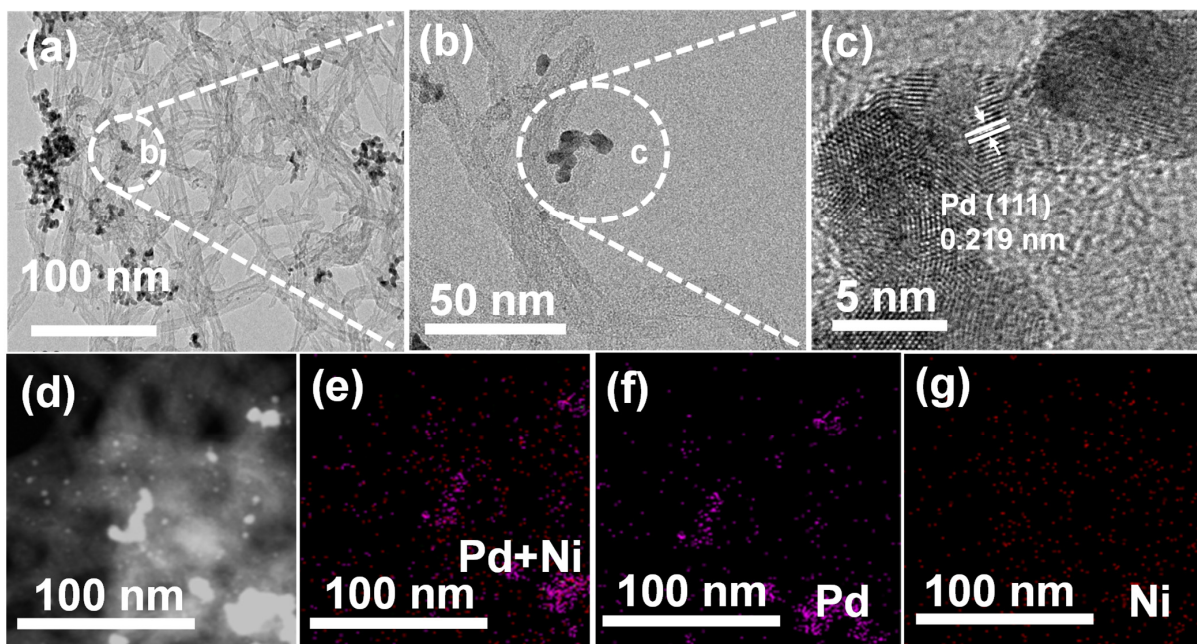


Figure 2. (a,b) TEM and (c) HRTEM images; (d–g) HAADF-STEM elements mapping, the corresponding elements Pd and Ni of Pd₂Ni₁/CNTs.

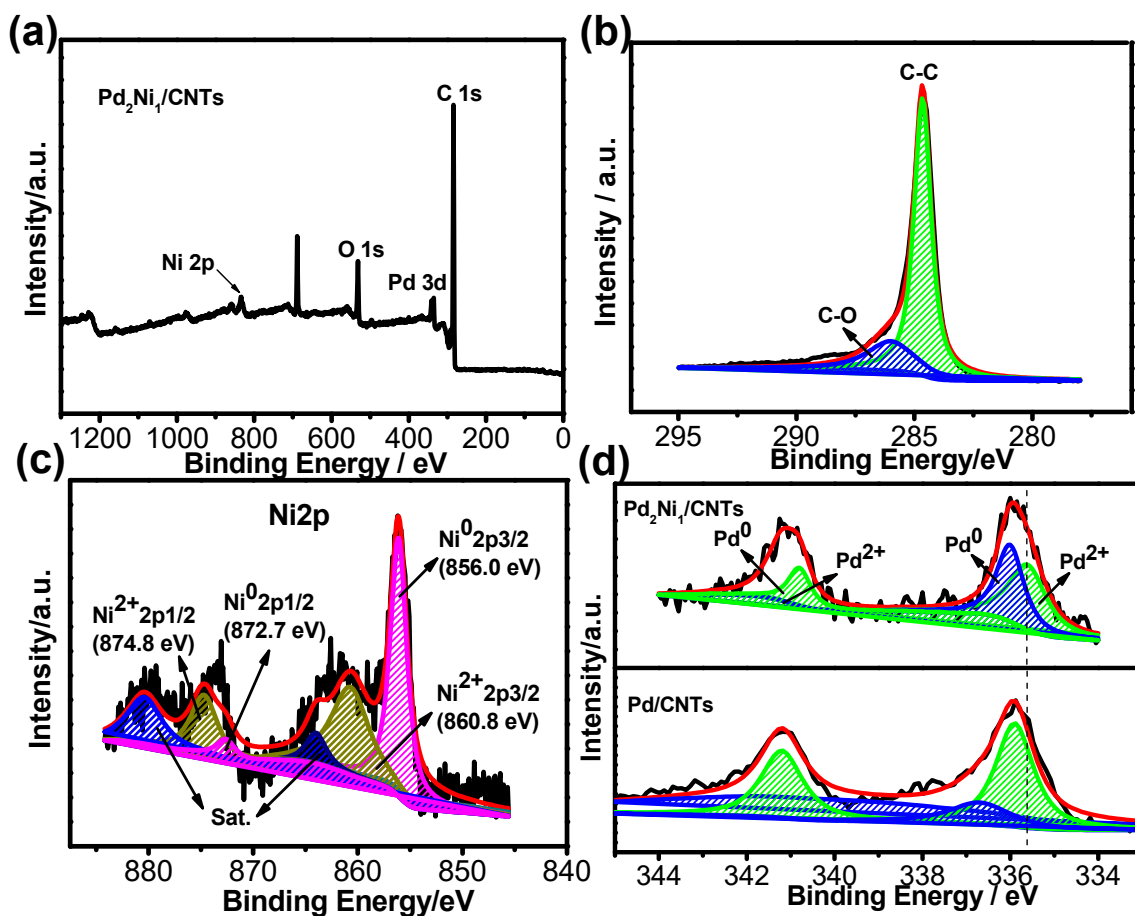


Figure 3. (a) XPS survey spectra, (b) C (1s) spectrum, (c) Ni (2p) spectrum of Pd₂Ni₁/CNTs, (d) Pd (3d) spectrum of Pd₂Ni₁/CNTs and Pd/CNTs.

As shown in Figure 4a, the ECSAs of Pd₂Ni₁/CNTs, Pd/CNTs, and Pd/C were calculated to be 53.30 m² g⁻¹, 42.70 m² g⁻¹, and 40.32 m² g⁻¹, which are most likely due to the Pd₂Ni₁ structural advantages. Larger ECSA is one of the reasons for the excellent activity of Pd₂Ni₁/CNTs, but it is not the main one. In order to obtain more suitable Ni doping, we optimized the atomic ratio of Pd to Ni (Figure 4b). The FAOR current densities of Pd₂Ni₁/CNTs, Pd₁Ni₁/CNTs, Pd₁Ni₂/CNTs, Pd/CNTs, and Pd/C are 3351.6 mA mg_{Pd}⁻¹, 1832.1 mA mg_{Pd}⁻¹, 1023.5 mA mg_{Pd}⁻¹, 2399.7 mA mg_{Pd}⁻¹, and 810.5 mA mg_{Pd}⁻¹ (Figure 4b,c). Obviously, Pd₂Ni₁/CNTs shows the highest catalytic activity. This phenomenon shows that appropriate Ni doping is necessary, and optimized Ni doping can effectively regulate the exonuclear electron configuration of Pd and thus affect the activity of catalyst. We performed a two-hour stability test on these catalysts (Figure 4d). All curves exhibit significant current attenuation at the initial stage, which was attributed to the formation of toxic species [35]. Finally, the Pd₂Ni₁/CNTs maintained excellent performance: 167.6 mA mg_{Pt}⁻¹ is almost 4.5 and 19.5 times greater compared to the values of Pd/CNTs, 37.2 mA mg_{Pt}⁻¹ and 8.6 mA mg_{Pt}⁻¹ for Pd/C, respectively. This phenomenon shows that Ni doping successfully inhibits the aggregation and shedding of active components in the catalyst. Good corrosion resistance of acidified MWCNTs was also demonstrated. These results above illustrate that Pd₂Ni₁/CNTs exhibits higher electrocatalytic activity and stability. Additionally, the Pd₂Ni₁/CNTs catalyst presents superior FAO mass activity in comparison to the Pd-based catalysts investigated in recent studies, as shown in Table S2. After CA investigations, the size of nanoparticles in Pd₂Ni₁/CNTs is still much smaller (3.8 nm) than that in Pd/CNTs (6.8 nm), as shown in Figure S4. This again demonstrates that the Pd₂Ni₁/CNTs catalyst exhibits excellent stability towards FAOR in the acidic environments. This phenomenon is attributed to the fact that the addition of Ni can change the electron configuration of Pd to produce a Pd–Ni bond to prevent the agglomeration of Pd in the electrocatalytic process. In addition, the surface of MWCNT-coated Pd–Ni nanoparticles contains more active sites, which helps to reduce the surface energy of Pd deposition and makes Pd more evenly dispersed.

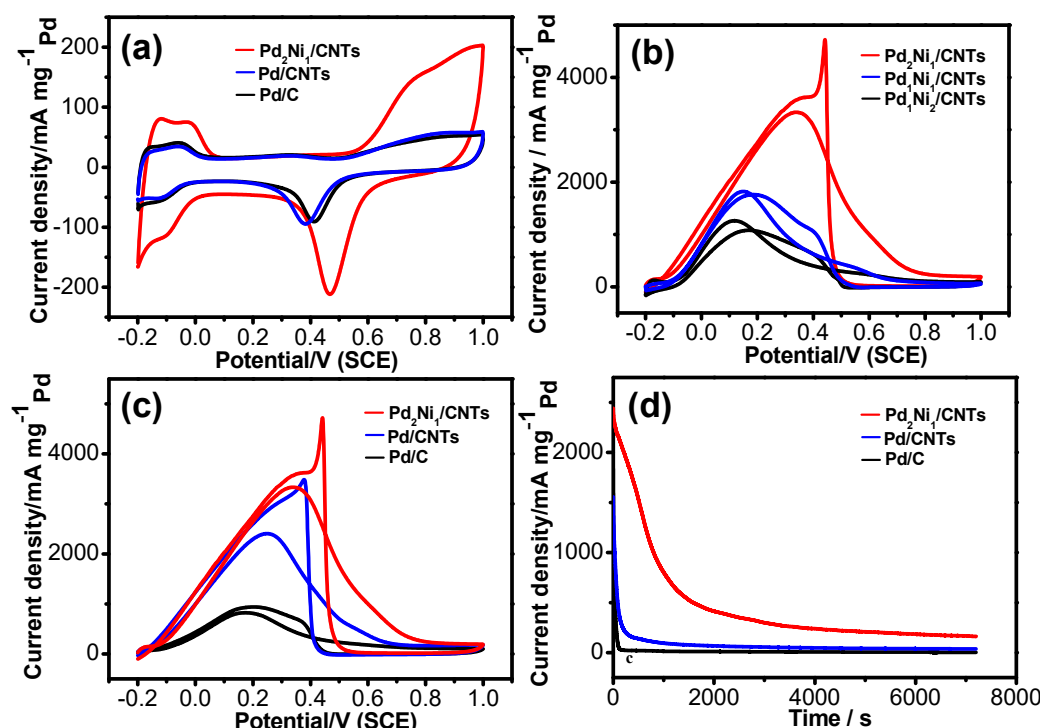


Figure 4. (a,c) Cyclic voltammograms and (d) current–time curves of Pd₂Ni₁/CNTs, Pd/CNTs, and Pd/C; (b) cyclic voltammograms curves of Pd₂Ni₁/CNTs, Pd₁Ni₁/CNTs, and Pd₁Ni₂/CNTs in 0.5 M H₂SO₄/1.0 M HCOOH + 0.5 M H₂SO₄ solution.

CO stripping experiments were conducted to test the anti-toxicity of these catalysts (Figure 5). Compared with Pd/CNTs (0.69V) and Pd/C (0.74V), the initial potential of CO oxidation adsorbed by Pd₂Ni₁/CNTs moved negatively to 0.66V, indicating that Pd₂Ni₁/CNTs has excellent CO oxidation ability, which is attributed to Ni doping. These newly added Ni sites can obtain more oxygen-containing groups (OH⁻) from H₂O and can release more effectively at active sites to improve CO tolerance [35]. This is also the main reason that the catalyst activity has been greatly improved.

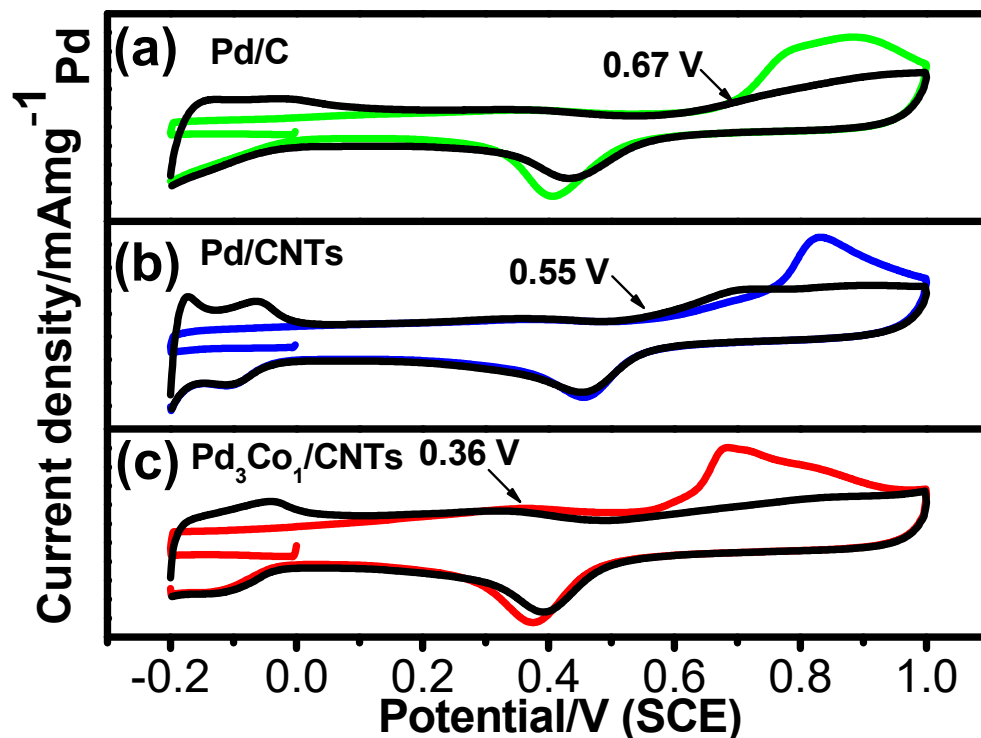


Figure 5. CO stripping voltammograms of Pd/C (a), Pd/CNTs (b), and Pd₂Ni₁/CNTs (c) catalysts in 0.5 M H₂SO₄ solution.

High catalytic activity and robust stability are the keys of DFAFC catalysts. Objectively, the catalytic activity and stability of the Pd₂Ni₁/CNTs catalyst prepared by us can only be described as relatively modest. Here are some possible explanations for the result. (1) Carrier CNTs were corroded in an acidic environment, resulting in separation of carrier and catalytic active component alloy NPs. (2) During the operation of the battery, the active components on the carrier may agglomerate or fall off, which may also be one of the reasons for the reduced activity and stability of the catalyst. (3) Catalyst poisoning caused by intermediates (such as CO_{ads}) produced during the reaction will also lead to degradation of catalyst performance and stability.

There are several methods to improve the activity of catalysts: (1) modification of carbon materials to improve their corrosion resistance, including non-covalent bonding, doping, or repairing defective carbon materials; (2) too add another metal to form a high entropy alloy helps to mitigate the toxicity (CO_{ads}). Therefore, the activity of the Pd₂Ni₁/CNTs catalyst still needs to be improved for better application in DFAFC.

3. Experimental

3.1. Materials

DES (choline chloride/oxalic acid) was prepared by referring to the literature [36]. MWCNT (OD: 10–20 nm, length: ~50 nm, purity > 95 wt%) was purchased from Nanjing Xianfeng Nanomaterial Technology Co., Ltd. Nafion solution (5 wt%) was purchased from Sigma-Aldrich. Choline chloride, oxalic acid, ethanol, PdCl₂, Ni(NO₃)₂, H₂SO₄, and HNO₃

were purchased from Shanghai Chemical Reagent Co., Ltd. (Shanghai, China), and all of the reagents were analytically pure.

3.2. Preparation of Catalysts

In general, a mixture of H_2SO_4 (60 mL) and HNO_3 (20 mL), with a volume ratio of 3 to 1, was used to acidify and functionalize MWCNT (1.0 g) (MWCNTs-AO) [37]. An amount of 20 mg MWCNTs-AO, 1.32 mL PdCl_2/DES solution (5 mg/mL), and 0.44 mL $\text{Ni}(\text{NO}_3)_2/\text{DES}$ solution (5 mg/mL) were added to 10 mL DES. Then, this mixture was stirred for three hours at room temperature. The obtained product was washed, with suction filtration, and vacuum dried at 60 °C (referring to $\text{Pd}_2\text{Ni}_1/\text{CNTs}$). In the control experiment, $\text{Pd}_1\text{Ni}_1/\text{CNTs}$, $\text{Pd}_1\text{Ni}_2/\text{CNTs}$, and Pd/CNTs were fabricated. All of the solutions were prepared using DES.

3.3. Physical Characterization

The X-ray diffraction (XRD) patterns were obtained using a X-ray diffractometer (Rigaku D/MAX 2500 v/pc, Japan), with Cu and K as radiation sources ($1\frac{1}{4}$ 1.5406 Å). The X-ray photoelectron spectroscopy (XPS) measurements were carried out using a Physical Electronics PHI Quantum 2000 system, with Al and K as radiation sources, and all of the XPS spectra were calibrated with the C1s line at 284.5 eV. The surface morphologies and microstructures of the prepared catalysts were analyzed using a high-resolution transmission electron microscope (HRTEM, JEOL JEM-2100) with an accelerating voltage of 200 kV. An inductively coupled plasma–optical emission spectrophotometer (ICP-OES, Thermo Electron IRIS Intrepid II XSP, USA) was used to characterize the morphology and content of these catalysts. The Pd contents in Pd/C (20%), Pd/CNTs (16.3%), $\text{Pd}_1\text{Ni}_1/\text{CNTs}$ (19.1%), $\text{Pd}_1\text{Ni}_2/\text{CNTs}$ (18.7%), and $\text{Pd}_2\text{Ni}_1/\text{CNTs}$ (18.6%) were measured (Table S3).

3.4. Electrochemical Measurements

The traditional three-electrode system of the electrochemical workstation was used for all electrochemical measurements. Platinum foil and a saturated calomel electrode (SCE) were used as the counter and reference electrodes, respectively. The working electrode was modified as follows: glass carbon electrode (GC, $\Phi = 5$ mm), 0.05 μm , 0.3 μm , and 1.0 μm alumina powder for polishing and processing. Then, the GC was cleaned with water and ethanol. A 2 mg catalyst was dispersed in a 1 mL solution, including 950 μL redistilled water and 50 μL Nafion solution (0.5 wt%). A 10 μL suspension was dripped over the GC electrode at room temperature. The Pd loading of Pd/C , Pd/CNTs , $\text{Pd}_1\text{Ni}_1/\text{CNTs}$, $\text{Pd}_1\text{Ni}_2/\text{CNTs}$, and $\text{Pd}_2\text{Ni}_1/\text{CNTs}$ were 24.6, 24.3, 25.3, 24.6, and 25.1 $\mu\text{g cm}^{-2}$.

These electrocatalytic behaviors were examined in 0.5 M H_2SO_4 and 1.0 M $\text{HCOOH} + 0.5$ M H_2SO_4 solution. For the CO anti-toxicity test, the CO was first bubbled in H_2SO_4 solution for 20 min at -0.2 – 0.0 V voltage scanning to make the working electrode completely poisoned. N_2 was then bubbled through the solution for 30 min to remove the CO in the solution. Keep N_2 above the solution at all times to prevent air interference.

4. Conclusions

Herein, we used DES as reducing agent, dispersant, and solvent to obtain $\text{Pd}_2\text{Ni}_1/\text{CNTs}$ catalyst, which shows excellent electrocatalytic performance and excellent anti-CO ability compared to $\text{Pd}_1\text{Ni}_1/\text{CNTs}$, $\text{Pd}_1\text{Ni}_2/\text{CNTs}$, Pd/CNTs , and Pd/C . The result is attributed to the virtue of compositional and structural advantages, which are benefits from the special DES. The special nanocluster structures of the Pd_2Ni_1 alloy lead to larger ESCA, and optimized Ni doping can effectively regulate the arrangement of the electron configuration of Pd, which effectively inhibits the adsorption of CO_{ads} on the active site. More OH^- obtained from Ni atoms can further interact with toxic intermediates to release more effective active sites. This study provides a new way (DES-assisted method) to fabricate Pd–Ni catalysts for fuel cells.

Supplementary Materials: The following supporting information can be downloaded at: <https://www.mdpi.com/article/10.3390/nano13040755/s1>, Figure S1: The corresponding particle size distribution of Pd/CNTs; Figure S2: TEM and HRTEM images of Pd/CNTs; Figure S3: EDX line-profiles (a), spot scanning (b) of Pd₂Ni₁ nanoparticle (where Pd is in red and Ni in blue) of Pd₂Ni₁/CNTs; Figure S4: TEM and HRTEM images; HAADF-STEM elements mapping; the corresponding elements Pd and Ni of Pd₂Ni₁/CNTs (another region); Table S1: Pd 3d peaks of Pd₂Ni₁/CNTs and Pd/CNTs; Table S2: A recent literatures survey of the activity of FAOR electrocatalysts; Table S3: Elemental composition of the samples obtained from ICP. References [35,38–46] are cited in the supplementary materials.

Author Contributions: Conceptualization, P.Y.; methodology, L.Z.; software, L.Z.; validation, S.D.; formal analysis, X.W.; investigation, X.W.; resources, W.C.; data curation, D.M.; writing—original draft preparation, P.Y.; writing—review and editing, Y.O.; visualization, X.W.; supervision, Y.X.; project administration, Y.X.; funding acquisition, J.F. All authors have read and agreed to the published version of the manuscript.

Funding: This research was funded by the Key Project of Hunan Provincial Education Department of China (22A0551) (Yuejun Ouyang), the Natural Science Foundation of Hunan Province (2020JJ4073) (Yuejun Ouyang), and the Hunan Provincial general project of the Education Department (21C0645) (Pingping Yang). This work was a key project of Huaihua University (HHUY2021-03) (Pingping Yang).

Institutional Review Board Statement: Not applicable.

Informed Consent Statement: Not applicable.

Data Availability Statement: Please contact Yixi Xie, xieyixige@xtu.edu.cn.

Acknowledgments: The Key Project of Hunan Provincial Education Department of China (22A0551), the Natural Science Foundation of Hunan Province (2020JJ4073), and the Hunan Provincial general project of the Education Department (21C0645). This work was a key project of Huaihua University (HHUY2021-03).

Conflicts of Interest: The authors declare no conflict of interest.

References

1. Liu, S.; Geng, S.; Li, L.; Zhang, Y.; Ren, G.; Huang, B.; Hu, Z.; Lee, J.F.; Lai, Y.H.; Chu, Y.H.; et al. A top-down strategy for amorphization of hydroxyl compounds for electrocatalytic oxygen evolution. *Nat. Commun.* **2022**, *13*, 1187. [CrossRef] [PubMed]
2. Tao, L.; Huang, B.; Jin, F.; Yang, Y.; Luo, M.; Sun, M.; Liu, Q.; Gao, F.; Guo, S. Atomic PdAu Interlayer Sandwiched into Pd/Pt Core/Shell Nanowires Achieves Superstable Oxygen Reduction Catalysis. *ACS Nano* **2020**, *14*, 11570–11578. [CrossRef] [PubMed]
3. Xiong, Y.; Dong, J.; Huang, Z.Q.; Xin, P.; Chen, W.; Wang, Y.; Li, Z.; Jin, Z.; Xing, W.; Zhuang, Z.; et al. Single-atom Rh/N-doped carbon electrocatalyst for formic acid oxidation. *Nat. Nanotechnol.* **2020**, *15*, 390–397. [CrossRef] [PubMed]
4. Li, X.; Gan, M.; Ma, L.; Zhao, W.; Zhang, Y.; Wang, L.; Hua, X. Facile synthesis of N-doped carbon nanotubes grafted on N-doped carbon nanosheets co-encapsulating cobalt and molybdenum carbide nanoparticles for efficient methanol oxidation. *Mater. Today Chem.* **2022**, *23*, 100665. [CrossRef]
5. Lu, Q.; Li, J.; Eid, K.; Gu, X.; Wan, Z.; Li, W.; Al-Hajri, R.S.; Abdullah, A.M. Facile one-step aqueous-phase synthesis of porous PtBi nanospheres for efficient electrochemical methanol oxidation with a high CO tolerance. *J. Electroanal. Chem.* **2022**, *916*, 116361. [CrossRef]
6. Yang, P.; Zhang, L.; Wei, X.; Dong, S.; Ouyang, Y. Pd₃Co₁ Alloy Nanocluster on the MWCNT Catalyst for Efficient Formic Acid Electro-Oxidation. *Nanomaterials* **2022**, *12*, 4182. [CrossRef]
7. Hu, Y.; Chen, C.; Shen, T.; Guo, X.; Yang, C.; Wang, D.; Zhu, Y. Hollow Carbon Nanorod Confined Single Atom Rh for Direct Formic Acid Electrooxidation. *Adv. Sci.* **2022**, *9*, e2205299. [CrossRef]
8. Al-Qodami, B.A.; Alalawy, H.H.; Al-Akraa, I.M.; Sayed, S.Y.; Allam, N.K.; Mohammad, A.M. Surface engineering of nanotubular ferric oxyhydroxide “goethite” on platinum anodes for durable formic acid fuel cells. *Int. J. Hydrogen Energy* **2022**, *47*, 264–275. [CrossRef]
9. Pramanick, B.; Kumar, T.; Chowdhury, S.; Halder, A.; Siril, P.F. Graphene-Supported Palladium Nanostructures as Highly Active Catalysts for Formic Acid Oxidation Reaction. *ACS Appl. Energy Mater.* **2022**, *5*, 13480–13491. [CrossRef]
10. Yang, L.; Wang, Y.; Feng, H.; Zeng, H.; Tan, C.; Yao, J.; Zhang, J.; Jiang, L.; Sun, Y. PdAg Nanoparticles with Different Sizes: Facile One-Step Synthesis and High Electrocatalytic Activity for Formic Acid Oxidation. *Chem. Asian J.* **2021**, *16*, 34–38. [CrossRef]
11. Chen, D.; Pei, S.; He, Z.; Shao, H.; Wang, J.; Wang, K.; Wang, Y.; Jin, Y. High Active PdSn Binary Alloyed Catalysts Supported on B and N Codoped Graphene for Formic Acid Electro-Oxidation. *Catalysts* **2020**, *10*, 751. [CrossRef]
12. Ulas, B.; Caglar, A.; Kivrak, H. Determination of optimum Pd:Ni ratio for Pd_xNi_{100-x}/CNTs formic acid electrooxidation catalysts synthesized via sodium borohydride reduction method. *Int. J. Energy Res.* **2019**, *43*, 3436–3445. [CrossRef]

13. Gharib, A.; Arab, A. Electrodeposited Pd, Pd Cd, and Pd Bi nanostructures: Preparation, characterization, corrosion behavior, and their electrocatalytic activities for formic acid oxidation. *J. Electroanal. Chem.* **2020**, *866*, 114166. [[CrossRef](#)]
14. Liu, S.; Wang, Z.; Zhang, H.; Yin, S.; Xu, Y.; Li, X.; Wang, L.; Wang, H. B-Doped PdRu nanopillar assemblies for enhanced formic acid oxidation electrocatalysis. *Nanoscale* **2020**, *12*, 19159–19164. [[CrossRef](#)]
15. Liu, X.; Bu, Y.; Cheng, T.; Gao, W.; Jiang, Q. Flower-like carbon supported Pd–Ni bimetal nanoparticles catalyst for formic acid electrooxidation. *Electrochim. Acta* **2019**, *324*, 134816. [[CrossRef](#)]
16. Li, M.; Liu, R.; Han, G.; Tian, Y.; Chang, Y.; Xiao, Y. Facile Synthesis of Pd–Ni Nanoparticles on Reduced Graphene Oxide under Microwave Irradiation for Formic Acid Oxidation. *Chin. J. Chem.* **2017**, *35*, 1405–1410. [[CrossRef](#)]
17. Zhang, W.; Yao, Q.; Wu, X.; Fu, Y.; Deng, K.; Wang, X. Intimately coupled hybrid of graphitic carbon nitride nanoflakelets with reduced graphene oxide for supporting Pd nanoparticles: A stable nanocatalyst with high catalytic activity towards formic acid and methanol electrooxidation. *Electrochim. Acta* **2016**, *200*, 131–141. [[CrossRef](#)]
18. Qian, H.; Wu, J.; Guo, Y.; Fang, W. PdAgPt Corner-Satellite Nanocrystals in Well-Controlled Morphologies and the Structure-Related Electrocatalytic Properties. *Nanomaterials* **2021**, *11*, 340. [[CrossRef](#)] [[PubMed](#)]
19. Saadat, N.; Dhakal, H.N.; Tjong, J.; Jaffer, S.; Yang, W.; Sain, M. Recent advances and future perspectives of carbon materials for fuel cell. *Renew. Sustain. Energy Rev.* **2021**, *138*, 110535. [[CrossRef](#)]
20. Li, Y.-H.; Deng, H.-C.; Zhou, Z.-H.; Yang, P.-P.; Fei, J.-J.; Xie, Y.-X. Pd12Ag1 nanoalloy on dendritic CNFs catalyst for boosting formic acid oxidation. *Appl. Surf. Sci.* **2023**, *608*, 155131. [[CrossRef](#)]
21. Wagle, D.V.; Zhao, H.; Baker, G.A. Deep Eutectic Solvents: Sustainable Media for Nanoscale and Functional Materials. *Acc. Chem. Res.* **2014**, *47*, 2299–2308. [[CrossRef](#)] [[PubMed](#)]
22. Yang, P.; Zhou, Z.; Zheng, T.; Gu, C.; Gong, X.; Zhang, Y.; Xie, Y.; Yang, N.; Fei, J. A novel strategy to synthesize Pt/CNTs nanocatalyst with highly improved activity for methanol electrooxidation. *J. Electroanal. Chem.* **2021**, *897*, 115557. [[CrossRef](#)]
23. Yang, P.; Wei, L.; Xiao, X.; Zhou, Z.; Li, J.; Zhang, Y.; Xie, Y.; Yang, N.; Fei, J. Electrocatalytic oxidation of formic acid on Pd/CNTs nanocatalysts synthesized in special “non-aqueous” system. *J. Electroanal. Chem.* **2022**, *906*, 115980. [[CrossRef](#)]
24. Yang, P.; Devasenathipathy, R.; Xu, W.; Wang, Z.; Chen, D.-H.; Zhang, X.; Fan, Y.; Chen, W. Pt₁(CeO₂)_{0.5} Nanoparticles Supported on Multiwalled Carbon Nanotubes for Methanol Electro-oxidation. *ACS Appl. Nano Mater.* **2021**, *4*, 10584–10591. [[CrossRef](#)]
25. Yang, P.; Li, Y.; Chen, S.; Li, J.; Zhao, P.; Zhang, L.; Xie, Y.; Fei, J. One-step synthesis in deep eutectic solvents of Pt₃Sn₁-SnO₂ alloy nanopore on carbon nanotubes for boosting electro-catalytic methanol oxidation. *J. Electroanal. Chem.* **2021**, *887*, 115164. [[CrossRef](#)]
26. Wang, R.-X.; Fan, Y.-J.; Liang, Z.-R.; Zhang, J.-M.; Zhou, Z.-Y.; Sun, S.-G. PdSn nanocatalysts supported on carbon nanotubes synthesized in deep eutectic solvents with high activity for formic acid electrooxidation. *RSC Adv.* **2016**, *6*, 60400–60406. [[CrossRef](#)]
27. Hung, T.-C.; Liu, Y.-R.; Chou, P.-C.; Lin, C.-W.; Hsieh, Y.-T. Electrochemical Sensing of Hydrazine Using Hollow Pd/Ag dendrites prepared by Galvanic replacement from Choline Chloride-based deep eutectic Solvents. *J. Electroanal. Chem.* **2022**, *922*, 116791. [[CrossRef](#)]
28. Hammons, J.A.; Muselle, T.; Ustarroz, J.; Tzedaki, M.; Raes, M.; Hubin, A.; Terryn, H. Stability, Assembly, and Particle/Solvent Interactions of Pd Nanoparticles Electrodeposited from a Deep Eutectic Solvent. *J. Phys. Chem. C* **2013**, *117*, 14381–14389. [[CrossRef](#)]
29. Bao, Y.; Zha, M.; Sun, P.; Hu, G.; Feng, L. PdNi/N-doped graphene aerogel with over wide potential activity for formic acid electrooxidation. *J. Energy Chem.* **2021**, *59*, 748–754. [[CrossRef](#)]
30. Tian, J.; Jiang, H.; Deng, X.; Zhao, X.; Tian, J.; Shi, G.; Li, G.; Zhang, J.; Zhang, W. Response modulation of PdNi nano-film hydrogen sensors by thickness control. *Appl. Surf. Sci.* **2021**, *562*, 150064. [[CrossRef](#)]
31. Kashif, M.; Quader, A.; Khan, M.A.; Ramay, S.M.; Atiq, S. Effectively coupled BiFeO₃-MnFe₂O₄-Cr₂O₃ tri-phase multiferroic composites for efficient energy storage and fast switching. *J. Alloy. Compd.* **2022**, *929*, 167274. [[CrossRef](#)]
32. Zhang, J.-M.; He, J.-J.; Wang, X.-Q.; Fan, Y.-J.; Zhang, X.-J.; Zhong, J.-P.; Chen, W.; Sun, S.-G. One-step synthesis in deep eutectic solvents of PtV alloy nanonetworks on carbon nanotubes with enhanced methanol electrooxidation performance. *Int. J. Hydrogen Energy* **2019**, *44*, 28709–28719. [[CrossRef](#)]
33. Wang, H.; Wang, W.; Mao, Q.; Yu, H.; Deng, K.; Xu, Y.; Li, X.; Wang, Z.; Wang, L. Tensile strained PdNi bimetallic for energy-efficient hydrogen production integrated with formate oxidation. *Chem. Eng. J.* **2022**, *450*, 137995. [[CrossRef](#)]
34. Li, X.; Wang, X.; Liu, M.; Liu, H.; Chen, Q.; Yin, Y.; Jin, M. Construction of Pd-M (M = Ni, Ag, Cu) alloy surfaces for catalytic applications. *Nano Res.* **2017**, *11*, 780–790. [[CrossRef](#)]
35. Zhang, L.Y.; Gong, Y.; Wu, D.; Wu, G.; Xu, B.; Bi, L.; Yuan, W.; Cui, Z. Twisted palladium-copper nanochains toward efficient electrocatalytic oxidation of formic acid. *J. Colloid Interface Sci.* **2019**, *537*, 366–374. [[CrossRef](#)] [[PubMed](#)]
36. Berjis, A.; Mirza, B.; Anaraki-Ardakani, H. One-Pot Synthesis of Highly Functionalized Indole in Choline Chloride/Oxalic Acid as a Deep Eutectic Solvent. *Polycycl. Aromat. Compd.* **2022**, 1–8. [[CrossRef](#)]
37. Zhang, L.; Li, J.; Wang, C.; Tang, J.; Chen, X.; Li, Y.; Shi, J.; Zhao, P.; Xie, Y.; Fei, J. A novel kaempferol electrochemical sensor based on glass carbon electrode modified by poly (3, 4-ethylenedioxythiophene) decorated with green synthesized MIL-100(Fe)-multi-walled carbon nanotubes composites. *Colloids Surfaces A Physicochem. Eng. Asp.* **2022**, *649*, 129484. [[CrossRef](#)]
38. Zhang, L.-Y.; Gong, Y.; Wu, D.; Li, Z.; Li, Q.; Zheng, L.; Chen, W. Palladium-cobalt nanodots anchored on graphene: In-situ synthesis, and application as an anode catalyst for direct formic acid fuel cells. *Appl. Surf. Sci.* **2019**, *469*, 305–311. [[CrossRef](#)]

39. Zhang, Z.; Gong, Y.; Wu, D.; Li, Z.; Li, Q.; Zheng, L.; Chen, W.; Yuan, W.; Zhang, L. Facile fabrication of stable PdCu clusters uniformly decorated on graphene as an efficient electrocatalyst for formic acid oxidation. *Int. J. Hydrogen Energy* **2019**, *44*, 2731–2740. [[CrossRef](#)]
40. Zheng, J.; Zeng, H.; Tan, C.; Zhang, T.; Zhao, B.; Guo, W.; Wang, H.; Sun, Y.; Jiang, L. Coral-like PdCu Alloy Nanoparticles Act as Stable Electrocatalysts for Highly Efficient Formic Acid Oxidation. *ACS Sustain. Chem. Eng.* **2019**, *7*, 15354–15360. [[CrossRef](#)]
41. Zhang, L.-Y.; Zhao, Z.; Yuan, W.; Li, C. Facile one-pot surfactant-free synthesis of uniform Pd₆Co nanocrystals on 3D graphene as an efficient electrocatalyst toward formic acid oxidation. *Nanoscale* **2016**, *8*, 1905–1909. [[CrossRef](#)] [[PubMed](#)]
42. Wang, L.; Zhai, J.; Jiang, K.; Wang, J.; Cai, W. Pd-Cu/C electrocatalysts synthesized by one-pot polyol reduction toward formic acid oxidation: Structural characterization and electrocatalytic performance. *Int. J. Hydrogen Energy* **2015**, *40*, 1726–1734. [[CrossRef](#)]
43. Sun, D.-D.; Si, L.; Fu, G.; Liu, C.; Sun, D.; Chen, Y.; Tang, Y.; Lu, T. Nanobranched porous palladium-tin intermetallics: One-step synthesis and their superior electrocatalysis towards formic acid oxidation. *J. Power Sources* **2015**, *280*, 141–146. [[CrossRef](#)]
44. Yang, F.; Zhang, Y.; Liu, P.; Cui, Y.; Ge, X.; Jing, Q. Pd-Cu alloy with hierarchical network structure as enhanced electrocatalysts for formic acid oxidation. *Int. J. Hydrogen Energy* **2016**, *41*, 6773–6780. [[CrossRef](#)]
45. Feng, A.-N.; Bai, J.; Shao, W.; Hong, W.; Tian, Z.; Xiao, Z. Surfactant-free Pd-Fe nanoparticles supported on reduced graphene oxide as nanocatalyst for formic acid oxidation. *Int. J. Hydrogen Energy* **2017**, *42*, 15196–15202.
46. Zhu, F.-C.; Ma, G.; Bai, Z.; Hang, R.; Tang, B.; Zhang, Z.; Wang, X. High activity of carbon nanotubes supported binary and ternary Pd-based catalysts for methanol, ethanol and formic acid electro-oxidation. *J. Power Sour.* **2013**, *242*, 610–620. [[CrossRef](#)]

Disclaimer/Publisher’s Note: The statements, opinions and data contained in all publications are solely those of the individual author(s) and contributor(s) and not of MDPI and/or the editor(s). MDPI and/or the editor(s) disclaim responsibility for any injury to people or property resulting from any ideas, methods, instructions or products referred to in the content.